
Two Sides of the Same Coin: Heterophily and Oversmoothing in Graph Convolutional Neural Networks

Yujun Yan¹ Milad Hashemi² Kevin Swersky² Yaoqing Yang³ Danai Koutra¹

Abstract

Most graph neural networks (GNN) perform poorly in graphs where neighbors typically have different features/classes (heterophily) and when stacking multiple layers (oversmoothing). These two seemingly unrelated problems have been studied independently, but there is recent empirical evidence that solving one problem may benefit the other. In this work, going beyond empirical observations, we theoretically characterize the connections between heterophily and oversmoothing, both of which lead to indistinguishable node representations. By modeling the change in node representations during message propagation, we theoretically analyze the factors (e.g., degree, heterophily level) that make the representations of nodes from different classes indistinguishable. Our analysis highlights that (1) nodes with high heterophily and nodes with low heterophily and low degrees relative to their neighbors (degree discrepancy) trigger the oversmoothing problem, and (2) allowing “negative” messages between neighbors can decouple the heterophily and oversmoothing problems. Based on our insights, we design a model that addresses the discrepancy in features and degrees between neighbors by incorporating signed messages and learned degree corrections. Our experiments on 9 real networks show that our model achieves state-of-the-art performance under heterophily, and performs comparably to existing GNNs under low heterophily (homophily). It also effectively addresses oversmoothing and even benefits from multiple layers.

1. Introduction

In recent years, graph neural networks or GNNs (Defferrard et al., 2016; Kipf & Welling, 2016; Veličković et al., 2017) have been used effectively in applications ranging from social science (Li & Goldwasser, 2019) and biology (Yan et al.,

¹University of Michigan ²Google Research ³University of California, Berkeley.

2019) to program understanding (Allamanis et al., 2018; Shi et al., 2019). A typical GNN architecture (Xu et al., 2018a) for the node classification task can be decomposed into two coarse steps: propagation/aggregation, and combination. Messages are first exchanged between neighboring nodes, then aggregated. Afterwards, the messages are combined with the self-representations (a.k.a., the current node representations) to update the node representations. Though GNNs are effective, they have some key limitations.

The first limitation is known as the “oversmoothing” problem (Li et al., 2018): the performance of GNNs degrade when stacking many layers. Recent work has found that oversmoothing could be caused by GNNs exponentially losing expressive power in the node classification task (Oono & Suzuki, 2019) and that the node representations converge to a stationary state which is decided by the degree of the nodes and the initial features (Chen et al., 2020; Wang et al., 2019; Rong et al., 2019; Rossi et al., 2020). These works focus on the analysis of the steady state in the limit of infinite layers, but they do not explore the dynamics on how oversmoothing is triggered, or which nodes tend to cause it. To date, works like (Xu et al., 2018b; Wang et al., 2019; Chen et al., 2020) have provided heuristic-based model designs to alleviate the oversmoothing problem. To fill in this gap, we seek to theoretically analyze the dynamics around oversmoothing.

The second limitation of GNNs is their poor performance on heterophily (or low-homophily) graphs (Pei et al., 2019; Zhu et al., 2020), which—unlike homophily graphs—have many neighboring nodes that belong to different classes (Newman, 2002). For instance, in protein networks, amino acids of different types tend to form links (Zhu et al., 2020), and in transaction networks, fraudsters are more likely to connect to accomplices than to other fraudsters (Pandit et al., 2007). Most GNNs (Kipf & Welling, 2016; Veličković et al., 2017) fail to effectively capture heterophily. Though emerging works have proposed some effective designs (Pei et al., 2019; Zhu et al., 2020), it remains an under-explored area.

These two limitations have mostly been studied independently, but recent work on oversmoothing (Chen et al., 2020) was shown empirically to address heterophily. Motivated by this empirical observation, we set out to understand the theoretical connection between the oversmoothing problem and

GNNs' poor performance on heterophily graphs by studying the change in node representations during message passing. Specifically, we make the following contributions:

- **Theory:** We investigate the dynamics of the node representations in the first and deeper layers. We model node features as random vectors and theoretically analyze the factors (e.g., degree, heterophily) that make the representations of nodes from different classes indistinguishable (oversmoothing).
- **Insights:** We find that (i) nodes with high heterophily and nodes with low heterophily & low degrees compared to their neighbors (degree discrepancy) trigger the oversmoothing problem; and (ii) allowing signed messages between neighbors can decouple the heterophily and oversmoothing problems.
- **Powerful model:** Based on these insights, we design a robust, generalized model, GGCN, that allows negative interactions between nodes and compensates for the effect of low-degree nodes through a learned rescaling scheme. Our empirical results show that our model is highly robust, achieving state-of-the-art performance on datasets with high levels of heterophily, and competitive performance on homophily datasets. Moreover, GGCN does not suffer from oversmoothing but rather improves or remains stable when stacking more layers.

2. Preliminaries

We first provide the notations and definitions that we use throughout the paper, and a brief background on GNNs.

Notation. We denote an unweighted and self-loop-free graph as $\mathcal{G}(\mathcal{V}, \mathcal{E})$ and its adjacency matrix as \mathbf{A} . We represent the degree of node $v_i \in \mathcal{V}$ by d_i , and the degree matrix—which is a diagonal matrix whose elements are node degrees—by \mathbf{D} . Let \mathcal{N}_i be the set of nodes directly connected to v_i , i.e., its neighbors. \mathbf{I} is the identity matrix.

We denote the node representations/features/output at l -th layer as \mathbf{F}^l and the weight matrix learned at the l -th layer as \mathbf{W}^l . Node v_i has a feature vector \mathbf{f}_i (the i -th row of \mathbf{F}) and l -th layer representation vector \mathbf{f}_i^l .

Homophily and Heterophily. Given a set of node labels / classes, the notion of *homophily* captures the tendency of a node to have the same class as its neighbors. Specifically, the homophily of node v_i is defined as $h_i = \mathbb{E}\left(\frac{|\mathcal{N}_i^s|}{|\mathcal{N}_i|}\right)$, where \mathcal{N}_i^s is the set of neighboring nodes with the same label as v_i , $|\cdot|$ is the cardinality operator, and the expectation is taken over the randomness of the node labels. High homophily corresponds to low heterophily, and vice versa, so we use these terms interchangeably throughout the paper.

Supervised Node Classification Task. We focus on node classification: Given a subset of labeled nodes (from a label set \mathcal{L}), the goal is to learn a mapping $\mathcal{F} : \mathbf{f}_i \mapsto \chi(v_i)$

between each node v_i and its ground truth label $\chi(v_i) \in \mathcal{L}$.

Graph Neural Networks. In general, for the node classification task, GNNs can be decomposed into two steps (Xu et al., 2018a): (1) neighborhood propagation and aggregation: $\hat{\mathbf{f}}_i^l = \text{AGGREGATE}(\mathbf{f}_j^l, v_j \in \mathcal{N}_i)$, and (2) combination: $\mathbf{f}_i^{l+1} = \text{COMBINE}(\hat{\mathbf{f}}_i^l, \mathbf{f}_i^l)$. The loss is given by $\text{CrossEntropy}(\text{softmax}(\mathbf{f}_i^l), \chi(v_i))$. A popular form of GNN is the Graph Convolutional Network (GCN). Among the various GCN variants (§ 6), the vanilla GCN model suggests a renormalization trick on the adjacency \mathbf{A} to prevent gradient explosion (Kipf & Welling, 2016). The $(l+1)$ -th output is given by: $\mathbf{F}^{l+1} = \sigma(\tilde{\mathbf{A}}\mathbf{F}^l\mathbf{W}^l)$, where $\tilde{\mathbf{A}} = \tilde{\mathbf{D}}^{-1/2}(\mathbf{I} + \mathbf{A})\tilde{\mathbf{D}}^{-1/2}$, $\tilde{\mathbf{D}}$ is the degree matrix of $\mathbf{I} + \mathbf{A}$, and σ is ReLU. An attention mechanism can be used to improve performance. For instance, the graph attention network (GAT) (Veličković et al., 2017) computes *nonnegative* attention weights on neighborhood nodes and replaces $\tilde{\mathbf{A}}$ with the learned attention weights.

3. Theoretical Analysis

In this section, we analyze the theoretical connections between the oversmoothing and heterophily problems. Unlike previous works (Chen et al., 2020; Wang et al., 2019) that study the final node representations in the limit of infinite layers, we focus on the *dynamic analysis of the node representations that are gradually passed to deeper layers*.

Setup. We consider a binary node classification task on an unweighted, self-loop-free graph \mathcal{G} with adjacency matrix \mathbf{A} . We denote the set of nodes in the first and second class as \mathcal{V}_1 and \mathcal{V}_2 , respectively. When $v_i \in \mathcal{V}_1$, \mathbf{f}_i^0 follows a distribution with mean $\boldsymbol{\mu}$ and variance $\boldsymbol{\Sigma}$, and when $v_i \in \mathcal{V}_2$, \mathbf{f}_i^0 follows a distribution with $-\boldsymbol{\mu}$ and $\boldsymbol{\Sigma}$. Our analysis uses GCN layers (§ 2) without nonlinearities and focuses on binary classification, but we demonstrate empirically that our results still apply to general settings (§ 5).

3.1. Heterophily & Oversmoothing

At a high level, our analysis highlights that both the oversmoothing problem and the heterophily problem result from *less linear separability* of learned representations for nodes in different classes after propagation and aggregation across layers. Specifically, our theory demonstrates that—in expectation—the layer-wise transformation of a node's representation depends on two factors: (1) the level of homophily (proportion of neighbors with the same class label), and (2) the relative degree of the node (how many neighbors it has relative to its neighbors). These factors determine if the node representation will tend to move towards the initial mean feature vector of the opposing class (become less linearly separable) or away (become more linearly separable). As shown in the left panel of Fig. 1, in more detail:

- In heterophily (low homophily) graphs, the decrease in

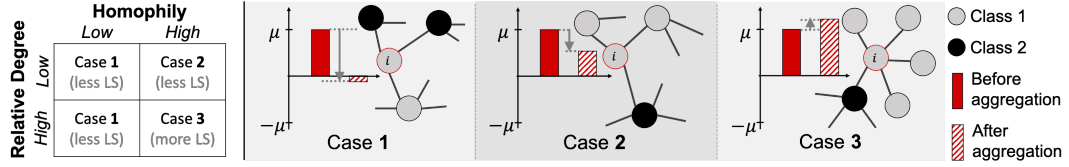


Figure 1. An illustration of node representation dynamics during neighborhood aggregation. The expectation of the representation from class 1 & 2 are denoted by μ and $-\mu$, respectively. The bars show the expected 1D node representations (scalars) of node v_i before and after the neighborhood aggregation. LS stands for linearly separability.

the linear separability is severe, causing performance drop even in shallow layers (case 1).

- In homophily graphs, high-degree nodes may initially benefit (case 3), leading to performance gain in shallow layers. However, the low-degree nodes eventually reduce the linear separability (case 2).

In more detail, the layer-wise message propagation and aggregation in GCNs is done via the $\tilde{\mathbf{A}}\mathbf{F}^l$ operation. Thus, for simplicity, our dynamic analysis investigates the impact of this operation on the node class and its relation to the level of homophily. However, the following conclusions still hold after scaling $\tilde{\mathbf{A}}\mathbf{F}^l$ by the learnable weight matrix \mathbf{W}^l . Next, we consider two stages: the *initial stage* at shallow layers of propagation and aggregation (§ 3.1), and the *developing stage* at deeper layers (§ 3.1).

. INITIAL STAGE: SHALLOW LAYERS

Theorem 1. [Initial Stage] During message passing in shallow layers, the nodes with **low homophily** $h_i \leq 0.5$ and the nodes with **high homophily** $h_i > 0.5$ but **small degree** d_i (w.r.t. their neighbors) are prone to be misclassified. Defining $r_{ij} \equiv \sqrt{\frac{d_i+1}{d_j+1}}$ and $\bar{r}_i \equiv \frac{1}{d_i} \sum_{j \in \mathcal{N}_i} r_{ij}$, the expectation of feature \mathbf{f}_i^1 after operation $\tilde{\mathbf{A}}\mathbf{F}^0$ at layer 1 is:

$$\mathbb{E}(\mathbf{f}_i^1) = \left(\frac{(2h_i - 1)d_i \bar{r}_i + 1}{d_i + 1} \right) \mathbb{E}(\mathbf{f}_i^0) \equiv \gamma_i^0 \mathbb{E}(\mathbf{f}_i^0), \quad (1)$$

$$\text{where } \gamma_i^0 \in \begin{cases} (-\infty, \frac{1}{2}], & \text{if } h_i \leq 0.5 \\ (\frac{1}{2}, 1], & \text{if } h_i > 0.5 \text{ \& } \bar{r}_i \leq \frac{1}{2h_i - 1} \\ (1, \infty), & \text{otherwise.} \end{cases} \quad (2)$$

For independent features \mathbf{f}_i^0 , the variance of each node is reduced to $\frac{1}{(d_i+1)} \left(\frac{1}{(d_i+1)} + \sum_{j \in \mathcal{N}_i} \frac{1}{(d_j+1)} \right) \Sigma \leq \frac{1}{2} \Sigma$.

Proof. We provide the proof in App. A.1. \square

Intuitively, under heterophily (case 1), the expected feature vector will move heavily towards the mean feature vector of the opposing class. For high homophily but low degrees (case 2), it will contract towards the origin. Otherwise, it will move away from the opposing class mean (case 3).

We note that our analysis shows that the variance of *each node* is reduced in the initial stage regardless of the homophily level. However, this does *not* mean that the variance of the nodes in the same *class* is reduced. The class variance is decided not only by the node variance but also how dispersed their mean is.

. DEVELOPING STAGE: DEEP LAYERS

Based on Eqs. (1)-(2), after propagation in several layers, the features of low-homophily nodes, and those of high-homophily but low-degree nodes may flip their sign. Assuming initial features \mathbf{f}_i^0 , propagation through l layers, and accumulated discount factor at the l -th layer $\gamma_i^l > 0$, we denote the sign-flipping features as $\mathbf{f}_i^l = -\gamma_i^l \mathbf{f}_i^0$, and the remaining features as $\mathbf{f}_i^l = \gamma_i^l \mathbf{f}_i^0$. We further define the **effective homophily** \hat{h}_i^l of node v_i as the ratio of the neighbors that have the same sign as v_i at the l -th layer. Similar to the analysis in the initial stage, we have:

Theorem 2. [Developing Stage] During message passing in deeper layers, when the effective homophily \hat{h}_i^l is sufficiently **low** ($\hat{h}_i^l \leq 0.5$), the **higher-degree nodes** (w.r.t. its neighbors) are prone to misclassification. Specifically, the expectation of the feature \mathbf{f}_i^{l+1} after the operation $\tilde{\mathbf{A}}\mathbf{F}^l$ at the $(l+1)$ -th layer is given by:

$$\mathbb{E}(\mathbf{f}_i^{l+1}) = \left(\frac{(2\hat{h}_i^l - 1)d_i \bar{r}_i + 1}{d_i + 1} \right) \gamma_i^l \mathbb{E}(\mathbf{f}_i^l). \quad (3)$$

Proof. The derivation is similar to that of Theorem 1 except that we replace the ground truth heterophily h_i with the effective heterophily \hat{h}_i^l and $\mathbb{E}(\mathbf{f}_i^l)$ with $\gamma_i^l \mathbb{E}(\mathbf{f}_i^l)$. Since graph \mathcal{G} is connected, the node degrees $d_i \geq 1$; thus, $\frac{d_i}{d_i+1}$ and \bar{r}_i are increasing functions of d_i , while $\frac{1}{d_i+1}$ is a decreasing function of d_i . When $\hat{h}_i^l \leq 0.5$, we have $(2\hat{h}_i^l - 1) \leq 0$, and $(2\hat{h}_i^l - 1) \cdot \frac{d_i}{d_i+1} \cdot \bar{r}_i + \frac{1}{d_i+1}$ is a decreasing function of d_i in Eq. (3). This suggests that the higher-degree nodes move towards the opposing class more. \square

We note that Eq. (3) also holds for layers $l \geq 2$ up to the layer when the effective homophily \hat{h}_i^l becomes smaller or equal to 0.5 for all the nodes. We regard these layers part of the initial stage, as they have three cases similar to Eq. (2).

. SUMMARY OF THEORETICAL RESULTS

Three conjectures follow from Theorems 1 and 2: (1) After message propagation, the mean vectors $\mathbb{E}(\mathbf{f}_i^1)$ will be dispersed. For a high-homophily graph, in the initial stage, the features of *low-degree nodes* (where $\bar{r}_i \ll \frac{1}{2h_i - 1}$) will first move towards the opposing class mean and have relatively lower accuracy (case 2). Later, when propagating to more layers, if the accuracy of low-degree nodes drops to a level such that the effective homophily of higher degree nodes satisfies $\hat{h}_i^l \leq 0.5$, then their features begin to move

towards the opposing class mean vector (case 1) because $(2\hat{h}_i^l - 1) \leq 0$ in Eq. (3).

(2) The message-passing based GNN model performs differently on graphs with different degree distributions. For homophily graphs with power-law distribution (with many low-degree nodes), the performance of low-degree nodes will degenerate fast in the initial stage and the model will quickly enter the developing stage. Then, due to few high-degree nodes, the performance will degenerate more slowly.

(3) The normalization scheme of the adjacency matrix of a graph makes a difference. The reason that node degrees appear in Eqs. (2)-(3) is the renormalization trick on \mathbf{A} in GCN (§ 2). Another normalization scheme such as row-normalization makes the scenario equivalent to a d -regular graph where nodes have the same degree (App. A.1).

3.2. Signed Messages for Heterophily & Oversmoothing

Attention-based GNN models (Veličković et al., 2017) typically use *non-negative* attention weights to discount the contribution from dissimilar neighbors. However, our theory highlights that signed messages are crucial for enhancing performance in heterophily graphs and alleviating the oversmoothing problem. Due to space limitations, we only show the effect of signed messages in the initial stage; similar results can be derived in the developing stage.

Setup. Consider the scenario where the “messages” sent by neighbors of a different class must be negated, and those by neighbors of the same class must be sent as-is. For node v_i , we define m_i^l as the *ratio of neighbors that send incorrect “messages”* at the l -th layer (i.e., different-class neighbors that send non-negated messages and same-class neighbors that send negated messages). We also define the l -th layer *error rate* as $e_i^l = \mathbb{E}(m_i^l)$, where the expectation is over the randomness of the neighbors that send incorrect messages. We make two assumptions: (1) Conditioned on m_i^l , whether the neighbor v_j will wrongly send the information is independent of its class $\chi(v_j)$; (2) The variable m_i^l is independent of the classes that nodes $v_j \in \mathcal{N}_i$ belong to.

Theorem 3. *With the independence assumptions and by allowing the messages to be optionally multiplied by a negative sign, in the initial stage, the mean distance between the nodes in different classes will **not be affected** by the initial homophily level h_i , but will be reduced by a **bigger error rate** e_i^l . Specifically, the multiplicative factor γ_i^0 after the operation $\tilde{\mathbf{A}}\mathbf{F}^0$ at first layer is given by:*

$$\mathbb{E}(\mathbf{f}_i^1) = \left(\frac{(1 - 2e_i^0)d_i\bar{r}_i + 1}{d_i + 1} \right) \mathbb{E}(\mathbf{f}_i^0) \equiv \gamma_i^0 \mathbb{E}(\mathbf{f}_i^0), \quad (4)$$

$$\text{where } \gamma_i^0 \in \begin{cases} (-\infty, \frac{1}{2}], & \text{if } e_i^0 \geq 0.5 \\ (\frac{1}{2}, 1], & \text{if } e_i^0 < 0.5 \text{ \& } \bar{r}_i \leq \frac{1}{1-2e_i^0} \\ (1, \infty), & \text{otherwise.} \end{cases} \quad (5)$$

Proof. A detailed proof is provided in App. A.2. \square

From Eq. (4), we conclude that: (1) Allowing neighbors of a different class to negate their messages prevents low homophily from degenerating performance. For a model that achieves low error rate at shallow layers (i.e., $e_i^0 \ll 0.5$), the low-degree nodes ($\bar{r}_i \ll \frac{1}{1-2e_i^0}$) trigger oversmoothing. (2) If a model does not work well under heterophily (i.e., high error rate e_i^l in identifying neighbors from other classes), it is prone to oversmoothing even in shallow layers.

4. Model Design

Based on our theoretical analysis, we propose two new, simple mechanisms to address both the heterophily and oversmoothing problems: signed messages and degree corrections. We integrate these mechanisms, along with a decaying combination of the current and previous node representations (Chen et al., 2020), into a robust, generalized GCN model, GGCN. In § 5, we empirically show its effectiveness in addressing the two closely-related problems.

4.1. Signed Messages

Theorem 3 points out the important role of signed messages in tackling the heterophily and oversmoothing problems. Our first proposed mechanism incorporates signed messages through cosine similarity between the nodes.

For expressiveness, as in GCN (Kipf & Welling, 2016), we first perform a learnable linear transformation of each node’s representation at the l -th layer: $\hat{\mathbf{F}}^l = \mathbf{F}^l \mathbf{W}^l + \mathbf{b}^l$, where \mathbf{b}^l is the bias vector at the l -th layer. Then, we define a sign function to be multiplied with the messages exchanged between neighbors. To allow for backpropagation of the gradient information, we approximate the sign function with a proxy, the correlation matrix of feature vectors without the self-correlation (i.e., \mathbf{I}):

$$\mathbf{S}^l = \frac{\hat{\mathbf{F}}^l \hat{\mathbf{F}}^{lT}}{\max(\text{diag}(\hat{\mathbf{F}}^l \hat{\mathbf{F}}^{lT}) \cdot \text{diag}(\hat{\mathbf{F}}^l \hat{\mathbf{F}}^{lT})^T, \delta)} - \mathbf{I},$$

where $\text{diag}(\cdot)$ is a column vector with the diagonal elements of the enclosed matrix, and δ is a very small constant (e.g., 10^{-9}) to prevent numerical instability. In addition to providing the necessary sign information, the correlation weights themselves provide more modeling flexibility.

In order to separate the contribution of similar neighbors (likely in the same class) from that of dissimilar neighbors (unlikely to be in the same class), we split \mathbf{S}^l into a positive matrix $\mathbf{S}_{\text{pos}}^l$ and a negative matrix $\mathbf{S}_{\text{neg}}^l$. Thus, our proposed GGCN model learns a weighted combination of the self-features, the positive messages, and the negative messages:

$$\mathbf{F}^{l+1} = \sigma \left(\hat{\alpha}^l (\hat{\beta}_0^l \hat{\mathbf{F}}^l + \hat{\beta}_1^l (\mathbf{S}_{\text{pos}}^l \odot \tilde{\mathbf{A}}) \hat{\mathbf{F}}^l + \hat{\beta}_2^l (\mathbf{S}_{\text{neg}}^l \odot \tilde{\mathbf{A}}) \hat{\mathbf{F}}^l) \right), \quad (6)$$

where $\hat{\beta}_0^l$, $\hat{\beta}_1^l$ and $\hat{\beta}_2^l$ are scalars obtained by applying soft-

max to the learned scalars β_0^l , β_1^l and β_2^l ; the non-negative scaling factor $\hat{\alpha}^l = \text{softplus}(\alpha^l)$ is derived from the learned scalar α^l ; \odot is element-wise multiplication; and σ is the nonlinear function Elu. We note that we learn *different* α and β parameters *per layer* for flexibility. We also require the combined weights, $\hat{\alpha}^l \hat{\beta}_x^l$, to be non-negative so that they do not negate the intended effect of the signed information.

4.2. Degree Corrections

Our analysis in § 3.2 highlights that, when allowing signed messages, oversmoothing is initially triggered by low-degree nodes. Thus, our second proposed mechanism aims to compensate for low degrees via degree corrections.

Based on Eq. (5), and given that most well-trained graph models have a relatively low error rate at the shallow layers (i.e., $e_i^l \ll 0.5$ for small l), we require that the node degrees satisfy $\bar{r}_i \geq \frac{1}{1-2e_i^0}$ to prevent oversmoothing. As we mentioned in § 3.1, the degrees appear in our theorems due to the renormalization trick on the adjacency matrix (§ 2). Since the node degrees cannot be modified, our strategy is to *rescale* them. Specifically, starting with the original formulation after a propagation at layer $l+1$:

$$(\tilde{A}\hat{\mathbf{F}}^l)[i,:] = \frac{\hat{\mathbf{F}}^l[i,:]}{d_i+1} + \sum_{v_j \in \mathcal{N}_i} \frac{\hat{\mathbf{F}}^l[j,:]}{\sqrt{d_i+1}\sqrt{d_j+1}}, \quad (7)$$

we correct the degrees by multiplying with scalars τ_{ij}^l :

$$(\tilde{A}\hat{\mathbf{F}}^l)[i,:] = \frac{\hat{\mathbf{F}}^l[i,:]}{d_i+1} + \sum_{v_j \in \mathcal{N}_i} \frac{\tau_{ij}^l \hat{\mathbf{F}}^l[j,:]}{\sqrt{d_i+1}\sqrt{d_j+1}}. \quad (8)$$

This multiplication is equivalent to changing the ratio r_{ij} in Thm. 1 to $\sqrt{\frac{(\tau_{ij}^l)^2(d_i+1)}{d_j+1}}$. That is, a larger τ_{ij}^l increases the effective \bar{r}_i at layer l .

Training independent τ_{ij}^l is not practical because it would require $O(|\mathcal{V}|^2)$ additional parameters per layer, which can lead to overfitting. Moreover, low-rank parameterizations suffer from unstable training dynamics. Intuitively, when r_{ij} is small, we would like to compensate for it via a larger τ_{ij}^l . Thus, we set τ_{ij}^l to be a function of r_{ij} as follows:

$$\tau_{ij}^l = \text{softplus} \left(\lambda_0^l \left(\frac{1}{r_{ij}} - 1 \right) + \lambda_1^l \right), \quad (9)$$

where λ_0^l and λ_1^l are learnable parameters. We subtract 1 so that when $r_{ij} = 1$ (i.e., $d_i = d_j$), then $\tau_{ij}^l = \text{softplus}(\lambda_1^l)$ is a constant bias.

In our proposed GGCN model, we combine the signed messages in Eq. (6) and our degree correction mechanism to obtain the features at layer $l+1$:

$$\mathbf{F}^{l+1} = \sigma \left(\hat{\alpha}^l \left(\hat{\beta}_0^l \hat{\mathbf{F}}^l + \hat{\beta}_1^l (\mathbf{S}_{\text{pos}}^l \odot \tilde{\mathbf{A}} \odot \mathbf{T}^l) \hat{\mathbf{F}}^l \right) \hat{\mathbf{F}}^l \right) \quad (10)$$

$$+ \hat{\beta}_2^l (\mathbf{S}_{\text{neg}}^l \odot \tilde{\mathbf{A}} \odot \mathbf{T}^l) \hat{\mathbf{F}}^l \right), \quad (11)$$

where \mathbf{T}^l is a matrix with elements τ_{ij}^l .

4.3. Decaying Aggregation

In addition to our two proposed mechanisms that are theoretically grounded in our analysis (§ 3), we also incorporate into GGCN an existing design—decaying aggregation of messages—that empirically increases performance. However, we note that, even without this design, our GNN architecture still performs well under heterophily and is robust to oversmoothing (§ 5.4).

Decaying aggregation was introduced in (Chen et al., 2020) as a way to slow down the convergence rate of node features in a K -layer GNN model with residual connections (Oono & Suzuki, 2019). Inspired by this work, we modify the decaying function, $\hat{\eta}$, and integrate it to our GGCN model:

$$\mathbf{F}^{l+1} = \mathbf{F}^l + \hat{\eta} \left(\sigma \left(\hat{\alpha}^l (\hat{\beta}_0^l \hat{\mathbf{F}}^l + \hat{\beta}_1^l (\mathbf{S}_{\text{pos}}^l \odot \tilde{\mathbf{A}} \odot \mathbf{T}^l) \hat{\mathbf{F}}^l \right) \hat{\mathbf{F}}^l \right. \right. \quad (12) \\ \left. \left. + \hat{\beta}_2^l (\mathbf{S}_{\text{neg}}^l \odot \tilde{\mathbf{A}} \odot \mathbf{T}^l) \hat{\mathbf{F}}^l \right) \right).$$

In practice, we found that the following decaying function works well: $\hat{\eta} \equiv \ln(\frac{\eta}{l^k} + 1)$, iff $l \geq l_0$; $\hat{\eta} = 1$, otherwise. The hyperparameters k , l_0 , η are tuned on the validation set.

4.4. Additional Considerations: Batch vs. Layer norm

Other mechanisms, such as batch or layer norm, may be seen as solutions to the heterophily and oversmoothing problems. However, batch norm cannot compensate for the dispersion of the mean vectors (§ 3) due to different degrees and homophily levels of the nodes. Although, to some extent, it reduces the speed by which the feature vectors of the susceptible nodes (case 1 & 2) move towards the other class (good for oversmoothing), it also prevents the feature vectors of the nodes that could benefit from the propagation (case 3) from increasing the distances (drop in accuracy). In our experiments (App. B.1), we find that, in general, adding batch norm significantly decreases the accuracy in heterophily datasets, but helps alleviate oversmoothing. Layer norm is a better option (Zhou et al., 2020) for oversmoothing and leads to a smaller decrease in accuracy than batch norm in most datasets. However, layer norm leads to a significant accuracy drop in some datasets when a subset of features are more important than the others.

5. Experiments

We aim to answer four questions: (Q1) Compared to the baselines, how does GGCN perform on homophily and heterophily graphs? (Q2) How robust is it against oversmoothing under homophily and heterophily? (Q3) How do different design choices affect its performance? (Q4) How does the performance for nodes with different degrees change with the number of layers in real datasets? (§ 3.1)

Table 1. Real data: mean accuracy \pm stdev over different data splits. Per GNN model, we report the best performance across different layers. Best model per benchmark highlighted in gray. The “ \dagger ” results (GraphSAGE) are obtained from (Zhu et al., 2020).

	Texas	Wisconsin	Actor	Squirrel	Chameleon	Cornell	Citeseer	Pubmed	Cora	Avg Rank
Hom. level h	0.11	0.21	0.22	0.22	0.23	0.3	0.74	0.8	0.81	
#Nodes	183	251	7,600	5,201	2,277	183	3,327	19,717	2,708	
#Edges	295	466	26,752	198,493	31,421	280	4,676	44,327	5,278	
#Classes	5	5	5	5	5	5	7	3	6	
GGCN (ours)	84.86 \pm 4.55	86.86 \pm 3.29	37.54 \pm 1.56	55.17 \pm 1.58	71.14 \pm 1.84	85.68 \pm 6.63	77.14 \pm 1.45	89.15 \pm 0.37	87.95 \pm 1.05	1.78
H2GCN*	84.86 \pm 7.23	87.65 \pm 4.98	35.70 \pm 1.00	36.48 \pm 1.86	60.11 \pm 2.15	82.70 \pm 5.28	77.11 \pm 1.57	89.49 \pm 0.38	87.87 \pm 1.20	3.44
GCNII*	77.57 \pm 3.83	80.39 \pm 3.4	37.44 \pm 1.30	38.47 \pm 1.58	63.86 \pm 3.04	77.86 \pm 3.79	77.33 \pm 1.48	90.15 \pm 0.43	88.37 \pm 1.25	3.11
Geom-GCN*	66.76 \pm 2.72	64.51 \pm 3.66	31.59 \pm 1.15	38.15 \pm 0.92	60.00 \pm 2.81	60.54 \pm 3.67	78.02 \pm 1.15	89.95 \pm 0.47	85.35 \pm 1.57	5.22
GraphSAGE \dagger	82.43 \pm 6.14	81.18 \pm 5.56	34.23 \pm 0.99	41.61 \pm 0.74	58.73 \pm 1.68	75.95 \pm 5.01	76.04 \pm 1.30	88.45 \pm 0.50	86.90 \pm 1.04	5.00
GCN	55.14 \pm 5.16	51.76 \pm 3.06	27.32 \pm 1.10	53.43 \pm 2.01	64.82 \pm 2.24	60.54 \pm 5.3	76.50 \pm 1.36	88.42 \pm 0.5	86.98 \pm 1.27	5.67
GAT	52.16 \pm 6.63	49.41 \pm 4.09	27.44 \pm 0.89	40.72 \pm 1.55	60.26 \pm 2.5	61.89 \pm 5.05	76.55 \pm 1.23	86.33 \pm 0.48	87.30 \pm 1.10	6.00
MLP	80.81 \pm 4.75	85.29 \pm 3.31	36.53 \pm 0.70	28.77 \pm 1.56	46.21 \pm 2.99	81.89 \pm 6.40	74.02 \pm 1.90	87.16 \pm 0.37	75.69 \pm 2.00	5.78

Table 2. Model performance for different layers: mean accuracy \pm stdev over different data splits. Per dataset and GNN model, we also report the layer at which the best performance (given in Table 1) is achieved. ‘OOM’: out of memory; ‘INS’: numerical instability.

Layers	2	4	8	16	32	64	Best	2	4	8	16	32	64	Best
Cora ($h=0.81$)														
GGCN (ours)	87.00 \pm 1.15	87.48 \pm 1.32	87.63 \pm 1.33	87.51 \pm 1.19	87.95 \pm 1.05	87.28 \pm 1.41	32	76.83 \pm 1.82	76.77 \pm 1.48	76.91 \pm 1.56	76.88 \pm 1.56	76.97 \pm 1.52	76.65 \pm 1.38	10
GCNII*	85.35 \pm 1.56	85.35 \pm 1.48	86.38 \pm 0.98	87.12 \pm 1.11	87.95 \pm 1.23	88.37 \pm 1.25	64	75.42 \pm 1.78	75.29 \pm 1.90	76.00 \pm 1.66	76.96 \pm 1.38	77.33 \pm 1.48	77.18 \pm 1.47	32
H2GCN*	87.87 \pm 1.20	86.10 \pm 1.51	86.18 \pm 2.10	OOM	OOM	OOM	2	76.90 \pm 1.80	76.09 \pm 1.54	74.10 \pm 1.83	OOM	OOM	OOM	1
Geom-GCN*	85.35 \pm 1.57	21.01 \pm 2.61	13.98 \pm 1.48	13.98 \pm 1.48	13.98 \pm 1.48	13.98 \pm 1.48	2	78.02 \pm 1.15	23.01 \pm 1.95	7.23 \pm 0.87	7.23 \pm 0.87	7.23 \pm 0.87	7.23 \pm 0.87	2
GAT	87.30 \pm 1.10	86.50 \pm 1.20	84.97 \pm 1.24	INS	INS	INS	2	76.55 \pm 1.23	75.33 \pm 1.39	66.57 \pm 5.08	INS	INS	INS	2
GCN	86.98 \pm 1.27	83.24 \pm 1.56	31.03 \pm 3.08	31.05 \pm 2.36	30.76 \pm 3.43	31.89 \pm 2.08	2	76.50 \pm 1.36	64.33 \pm 8.27	24.18 \pm 1.71	23.07 \pm 2.95	25.3 \pm 1.77	24.73 \pm 1.66	2
Cornell ($h=0.3$)														
GGCN (ours)	83.78 \pm 6.73	83.78 \pm 6.16	84.86 \pm 5.69	83.78 \pm 6.73	83.78 \pm 6.51	84.32 \pm 5.90	6	70.77 \pm 1.42	69.58 \pm 2.68	70.33 \pm 1.70	70.44 \pm 1.82	70.29 \pm 1.62	70.20 \pm 1.95	5
GCNII*	67.57 \pm 11.34	64.59 \pm 9.63	73.24 \pm 9.51	77.84 \pm 3.97	75.41 \pm 5.47	73.78 \pm 4.37	16	61.07 \pm 4.10	63.86 \pm 3.04	62.89 \pm 1.18	60.20 \pm 2.10	56.97 \pm 1.81	55.99 \pm 2.27	4
H2GCN*	81.89 \pm 9.98	82.70 \pm 6.27	80.27 \pm 6.63	OOM	OOM	OOM	1	59.06 \pm 1.85	60.11 \pm 1.15	OOM	OOM	OOM	OOM	4
Geom-GCN*	60.54 \pm 3.67	23.78 \pm 11.64	12.97 \pm 2.91	12.97 \pm 2.91	12.97 \pm 2.91	12.97 \pm 2.91	2	60.00 \pm 2.81	19.17 \pm 1.66	19.58 \pm 1.73	19.58 \pm 1.73	19.58 \pm 1.73	19.58 \pm 1.73	2
GAT	61.89 \pm 5.05	58.38 \pm 4.05	58.38 \pm 3.86	INS	INS	INS	2	60.26 \pm 2.50	48.71 \pm 2.96	35.09 \pm 3.55	INS	INS	INS	2
GCN	60.54 \pm 5.30	59.19 \pm 3.30	58.92 \pm 3.15	58.92 \pm 3.15	58.92 \pm 3.15	58.92 \pm 3.15	2	64.82 \pm 2.24	53.11 \pm 4.44	35.15 \pm 3.14	35.39 \pm 3.23	35.20 \pm 3.25	35.50 \pm 3.08	2
Chameleon ($h=0.23$)														

5.1. Experimental Setup

Datasets. We evaluate the performance of our GGCN model and existing GNNs in node classification on various real-world datasets (Tang et al., 2009; Rozemberczki et al., 2019; Sen et al., 2008; Namata et al., 2012; Bojchevski & Günnemann, 2018; Shchur et al., 2018). We provide their summary statistics in Table 1, where we compute the homophily level h of a graph as the average of h_i of all nodes $v_i \in \mathcal{V}$. For all benchmarks, we use the feature vectors, class labels, and 10 random splits (48%/32%/20% of nodes per class for train/validation/test¹) from (Pei et al., 2019).

Baselines. For baselines we use (1) classic GNN models for node classification: vanilla GCN (Kipf & Welling, 2016), GAT (Veličković et al., 2017) and GraphSage (Hamilton et al., 2017); (2) recent models tackling heterophily: Geom-GCN (Pei et al., 2019) and H2GCN (Zhu et al., 2020); (3) the state-of-the-art model for oversmoothing, GCNII (Chen et al., 2020); and (4) 2-layer MLP (with dropout and Elu non-linearity). For GCN, Geom-GCN, GCNII and H2GCN, we use the original codes provided by the authors. For GAT, we use the code from a well-accepted Github repository². For GraphSage, we report the results from (Zhu et al., 2020), which uses the same data and splits. For the baselines that have multiple variants (Geom-GCN, GCNII, H2GCN), we

¹(Pei et al., 2019) claims that the ratios are 60%/20%/20%, which is different from the actual data splits shared on GitHub.

²<https://github.com/Diego999/pyGAT>

choose the best variant for each dataset and denote them as [model]*. We set the same hyperparameters that are provided by the paper or the authors’ github repository, and we match their reported results if they used the same dataset and split as us. The hyperparameter settings for GGCN can be found in App. B.3.

Machine. We ran our experiments on Nvidia V100 GPU.

5.2. Q1. Performance Under Homophily & Heterophily

Table 1 provides the accuracy of different GNNs on the supervised node classification task over datasets with varying homophily levels (arranged from low homophily to high homophily). We report the best performance of each model across different layers.

We observe that GGCN performs the best in terms of average rank (1.78) across all datasets, which suggests its strong adaptability to graphs of various homophily levels. In particular, GGCN achieves the highest accuracy in 5 out of 6 heterophily graphs ($h \leq 0.5$). For datasets like Chameleon and Cornell, GGCN enhances accuracy by around 6% and 3% compared to the second-best model. On homophily datasets (Citeseer, Pubmed, Cora), the accuracy of GGCN is within a 1% difference of the best model.

Our experiments highlight that MLP is a good baseline in heterophily datasets. In heterophily graphs, the models that are not specifically designed for heterophily usually perform worse than an MLP. Though H2GCN* is the second

Table 3. Ablation study: degree correction has consistent benefits (robust to oversmoothing & ability to handle heterophily) in different datasets while signed information has more benefits in heterophily datasets. Best performance of each model is highlighted in gray.

Layers	2	4	8	16	32	64	2	4	8	16	32	64
Cora ($h=0.81$)												
Base	86.56 \pm 1.21	86.04 \pm 0.72	85.51 \pm 1.51	85.33 \pm 0.72	85.37 \pm 1.58	72.17 \pm 8.89	76.51 \pm 1.63	75.03 \pm 1.67	73.96 \pm 1.52	73.59 \pm 1.51	71.91 \pm 1.94	32.08 \pm 15.74
+deg	86.72 \pm 1.29	86.02 \pm 0.97	85.49 \pm 1.32	85.27 \pm 1.59	85.27 \pm 1.51	84.21 \pm 1.22	76.63 \pm 1.38	74.64 \pm 1.97	74.15 \pm 1.61	73.73 \pm 1.31	73.61 \pm 1.84	70.56 \pm 2.27
+sign	84.81 \pm 1.63	86.06 \pm 1.7	85.67 \pm 1.26	85.39 \pm 0.97	84.85 \pm 0.98	78.57 \pm 6.73	77.13 \pm 1.69	74.56 \pm 2.02	73.64 \pm 1.65	72.31 \pm 2.32	71.98 \pm 3.44	68.68 \pm 6.72
+deg, sign	86.96 \pm 1.38	86.20 \pm 0.89	85.63 \pm 0.78	85.47 \pm 1.18	85.55 \pm 1.66	77.81 \pm 7.95	76.81 \pm 1.71	74.68 \pm 1.97	74.69 \pm 2.35	73.28 \pm 1.45	71.81 \pm 2.28	69.91 \pm 3.97
Cornell ($h=0.3$)												
Base	61.89 \pm 3.72	60.00 \pm 5.24	58.92 \pm 5.24	56.49 \pm 5.73	58.92 \pm 3.15	49.19 \pm 16.70	64.98 \pm 1.84	62.65 \pm 3.09	62.43 \pm 3.28	54.69 \pm 2.58	47.68 \pm 2.63	29.74 \pm 5.21
+deg	63.78 \pm 15.57	62.70 \pm 5.90	59.46 \pm 4.52	56.49 \pm 5.73	57.57 \pm 4.20	58.92 \pm 3.15	66.54 \pm 2.19	68.31 \pm 2.70	68.99 \pm 2.38	67.68 \pm 3.7	56.86 \pm 8.8	41.95 \pm 9.56
+sign	85.41 \pm 7.27	76.76 \pm 7.07	70.00 \pm 5.19	67.57 \pm 9.44	63.24 \pm 6.07	63.24 \pm 6.53	65.31 \pm 3.2	53.55 \pm 6.35	53.05 \pm 2.28	51.93 \pm 4.00	57.17 \pm 3.39	51.93 \pm 8.95
+deg, sign	84.32 \pm 6.37	78.92 \pm 8.09	73.51 \pm 5.90	70.81 \pm 5.64	68.11 \pm 5.14	62.43 \pm 6.67	65.75 \pm 1.81	61.49 \pm 7.38	53.73 \pm 7.79	52.43 \pm 5.37	55.92 \pm 5.14	56.95 \pm 3.93
Citeseer ($h=0.74$)												
Chameleon ($h=0.23$)												

best model in heterophily datasets, we can still see that in the Actor dataset, MLP performs better. Geom-GCN*, which is specifically designed for heterophily, achieves better performance than classic GNNs (GCN and GAT), but it is outperformed by MLP on heterophily datasets (except Chameleon and Squirrel). Our GGCN model is the only model that performs better than MLP across all the datasets.

In general, GNN models perform well in homophily datasets. GCNII* performs the best, and GGCN, H2GCN*, and Geom-GCN* also achieve high performance.

5.3. Q2. Oversmoothing

We also test how robust the models are to oversmoothing. To this end, we measure the supervised node classification accuracy for 2 to 64 layers. Table 2 presents the results for two homophily datasets (top) and two heterophily datasets (bottom). Per model, we also report the layer at which the best performance is achieved (column ‘Best’).

According to Table 2, GGCN and GCNII* achieve **increase** in accuracy when stacking more layers. Models that are not designed for oversmoothing have various issues. The performance of GCN and Geom-GCN* drops rapidly as the number of layers grows; H2GCN* requires concatenating all the intermediate outputs and quickly reaches memory capacity; GAT’s attention mechanism also has high memory requirements. We also find that GAT needs careful initialization when stacking many layers as it may suffer from numerical instability in sparse tensor operations.

In general, models like GGCN, GCNII*, and H2GCN* that perform well under heterophily usually exhibit higher resilience against oversmoothing. One exception is Geom-GCN*, which suffers more than GCN. This model incorporates structurally similar nodes into each node’s neighborhood; this design may benefit Geom-GCN* in the shallow layers as the node degrees increase. However, as we point out in Thm. 2, when the effective homophily is low, higher degrees are harmful. If the structurally similar nodes introduce lower homophily levels, their performance will rapidly degrade once the effective homophily is lower than 0.5. On the other hand, GGCN *virtually* changes the degrees thanks to the degree correction mechanism (§ 4.2), and, in prac-

tice, this design has **positive** impact on its robustness to oversmoothing.

5.4. Q3. Ablation Study for the Proposed Mechanisms

We now study the impact of our two proposed mechanisms (signed messages and degree correction, presented in § 4). To better show their effects, we add each design choice to a base model and track the changes in the node classification performance. As the base model, we choose a GCN variant that uses the message passing mechanism (Kipf & Welling, 2016) with weight bias, a residual connection (but *not decaying aggregation*) for robustness to oversmoothing, and Elu non-linearity σ . We denote the model that replaces the message passing with our signed messages mechanism as **+sign**, and the model that incorporates the degree correction as **+deg**. The model that uses both designs is denoted as **+sign, deg**. Table 3 gives the accuracy of the models in the supervised node classification task for different layers.

We observe that both mechanisms alleviate the oversmoothing problem. Specifically, the base model has a sharp performance decrease after 32 layers, while the other models have significantly higher performance. In general, the **+deg** model is better than **+sign** in alleviating oversmoothing, and has a consistent performance gain across different data. For Chameleon, we observe increase in accuracy as we stack more layers; the large performance gain of GGCN results from the degree correction. In Cora and Cornell, **+sign, deg** consistently performs better across different layers than the model with only one design, demonstrating the constructive effect from our two proposed mechanisms.

The signed message design has an advantage in heterophily datasets. In the Cornell dataset, using signed information rather than plain message passing results in over 20% gain, which explains the strong performance of GGCN. However, in homophily datasets, the benefit from signed messages is limited, as these datasets have few different-class neighbors.

As we pointed out in Thm. 3, when signs are included, the error rate affects the performance. For the models that do not include signed messages, Thms. 1 and 2 indicate that the effective homophily level affects the performance. In order to achieve gain in performance, we need to make sure that

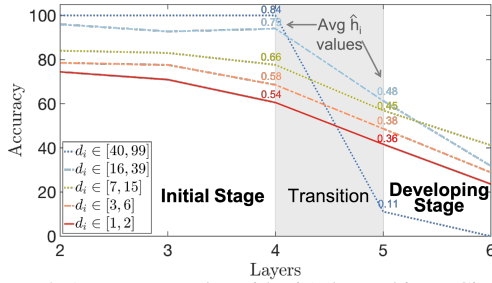


Figure 2. Accuracy per (logarithmic) degree bin on Citeseer. Initial stage: when average $\hat{h}_i \geq 0.5$, the accuracy increases as the degree increases. Developing stage: when average $\hat{h}_i < 0.5$, the accuracy of high-degree nodes decreases more sharply.

the error rate is lower than $1 - \hat{h}$. In the homophily datasets, since the effective homophily \hat{h} is high, the signed messages are not very beneficial. However, in the heterophily datasets, \hat{h} is low, and our proposed mechanism helps.

5.5. Q4. Case Study: Initial & Developing Stages

Using the vanilla GCN model (Kipf & Welling, 2016), we validate our theorems by measuring the accuracy and effective homophily for different node degrees (binned logarithmically) on real datasets. We estimate the effective homophily as the portion of the same-class neighbors that are correctly classified *before* the last propagation. Figure 2 shows the results for Citeseer; we see that initially the accuracy increases with the degree, but the trend changes when the average effective \hat{h}_i drops below 0.5, with high-degree nodes being impacted the most, as predicted by our theorems. We give details for this analysis in App. B.2.

6. Related Work

Graph Neural Networks. Early on, Defferrard et al. (2016) proposed a GNN model that combines spectral filtering of graph signals and non-linearity for supervised node classification. The scalability and numerical stability of GNNs was later improved with a localized first-order approximation of spectral graph convolutions proposed in (Kipf & Welling, 2016). Graph attention was introduced to improve the neighborhood aggregation step (Veličković et al., 2017). Veličković et al. (2017) proposes the first graph attention network to improve neighborhood aggregation. Many more GNN variants have been proposed for different applications such as: computer vision (Satorras & Estrach, 2018), social science (Li & Goldwasser, 2019), biology (Yan et al., 2019), algorithmic tasks (Veličković et al., 2020; Yan et al., 2020), and inductive classification Hamilton et al. (2017).

Oversmoothing. The oversmoothing problem was first discussed in (Li et al., 2018), which proved that by repeatedly applying Laplacian smoothing, the features of nodes within each connected component of the graph converge to the same value. Since then, various empirical solutions have been proposed: residual connections and dilated con-

volutions (Li et al., 2019); skip links (Xu et al., 2018b); new normalization strategies (Zhao & Akoglu, 2019); edge dropout (Rong et al., 2019); and a new model that even increases performance as more layers are stacked (Chen et al., 2020). Some recent works provide theoretical analyses: Oono & Suzuki (2019) showed that a k -layer renormalized graph convolution with a residual link simulates a lazy random walk and Chen et al. (2020) proved that the convergence rate is related to the spectral gap of the graph.

Heterophily & GNNs. Heterophily has recently been recognized as an important issue for GNNs. It is first outlined in the context of GNNs in (Pei et al., 2019). Zhu et al. (2020) identified a set of effective designs that allow GNNs to generalize to challenging heterophily settings, and Zhu et al. (2021) introduced a new GNN model that leverages ideas from belief propagation (Gatterbauer et al., 2015). Though recent work (Chen et al., 2020) focused on solving the oversmoothing problem, it also empirically showed improvement on heterophily datasets; these empirical observations formed the basis of our work. Finally, Chien et al. (2021) recently proposed a pagerank-based model that performs well under heterophily and alleviates the oversmoothing problem. However, they view the two problems independently, while our work provides theoretical and empirical connections.

Our Work. Our work lies at the intersection of the aforementioned areas. We theoretically and empirically unveil connections between the oversmoothing and heterophily problems. We also provide a new perspective to analyze these problems, and point out key factors that impact their interplay within the GCN message propagation dynamics.

7. Conclusion

Our work provides the first theoretical and empirical analysis that unveils the connections between the oversmoothing and heterophily problems. By modeling the node features as random vectors, we study the dynamics of message propagation in GCNs and analyze whether the vectors tend to move closer to/away from the other classes in expectation. Through this new perspective, we obtain two important insights: (1) nodes with high heterophily and nodes with low heterophily and low degrees compared to their neighbors (degree discrepancy) trigger the oversmoothing problem, and (2) allowing ‘negative’ messages between neighbors can decouple the heterophily and oversmoothing problems. Based on these insights, we design a robust model, GGCN, which simultaneously addresses the heterophily and oversmoothing problems. Though other designs may also address the two problems, our work points out two effective directions which are theoretically grounded (§ 3). How to effectively incorporate signed information, and jointly optimize signed information and degree corrections are still open problems worth further exploration.

References

Allamanis, M., Brockschmidt, M., and Khademi, M. Learning to represent programs with graphs, 2018.

Bojchevski, A. and Günnemann, S. Deep gaussian embedding of graphs: Unsupervised inductive learning via ranking. In *International Conference on Learning Representations (ICLR)*, 2018. URL <https://openreview.net/forum?id=r1ZdKJ-0W>.

Chen, M., Wei, Z., Huang, Z., Ding, B., and Li, Y. Simple and deep graph convolutional networks. In *International Conference on Machine Learning*, pp. 1725–1735. PMLR, 2020.

Chien, E., Peng, J., Li, P., and Milenkovic, O. Adaptive universal generalized pagerank graph neural network, 2021.

Defferrard, M., Bresson, X., and Vandergheynst, P. Convolutional neural networks on graphs with fast localized spectral filtering. In *Proceedings of the 30th International Conference on Neural Information Processing Systems*, pp. 3844–3852, 2016.

Gatterbauer, W., Günnemann, S., Koutra, D., and Faloutsos, C. Linearized and single-pass belief propagation. *Proc. VLDB Endow.*, 8(5):581–592, January 2015.

Hamilton, W. L., Ying, R., and Leskovec, J. Inductive representation learning on large graphs. In *Proceedings of the 31st International Conference on Neural Information Processing Systems*, pp. 1025–1035, 2017.

Kipf, T. N. and Welling, M. Semi-supervised classification with graph convolutional networks. *arXiv preprint arXiv:1609.02907*, 2016.

Li, C. and Goldwasser, D. Encoding social information with graph convolutional networks for political perspective detection in news media. In *Proceedings of the 57th Annual Meeting of the Association for Computational Linguistics*, pp. 2594–2604, 2019.

Li, G., Muller, M., Thabet, A., and Ghanem, B. Deepgcns: Can gcns go as deep as cnns? In *Proceedings of the IEEE/CVF International Conference on Computer Vision*, pp. 9267–9276, 2019.

Li, Q., Han, Z., and Wu, X.-M. Deeper insights into graph convolutional networks for semi-supervised learning. In *Proceedings of the AAAI Conference on Artificial Intelligence*, volume 32, 2018.

Namata, G., London, B., Getoor, L., Huang, B., and EDU, U. Query-driven active surveying for collective classification. In *10th International Workshop on Mining and Learning with Graphs*, volume 8, 2012.

Newman, M. E. Assortative mixing in networks. *Physical review letters*, 89(20):208701, 2002.

Oono, K. and Suzuki, T. Graph neural networks exponentially lose expressive power for node classification. In *International Conference on Learning Representations*, 2019.

Pandit, S., Chau, D. H., Wang, S., and Faloutsos, C. Netprobe: a fast and scalable system for fraud detection in online auction networks. In *Proceedings of the 16th international conference on World Wide Web*, pp. 201–210, 2007.

Pei, H., Wei, B., Chang, K. C.-C., Lei, Y., and Yang, B. Geom-gcn: Geometric graph convolutional networks. In *International Conference on Learning Representations*, 2019.

Rong, Y., Huang, W., Xu, T., and Huang, J. Dropedge: Towards deep graph convolutional networks on node classification. In *International Conference on Learning Representations*, 2019.

Rossi, R. A., Jin, D., Kim, S., Ahmed, N. K., Koutra, D., and Lee, J. B. On proximity and structural role-based embeddings in networks: Misconceptions, techniques, and applications. *ACM Trans. Knowl. Discov. Data*, 14(5), August 2020.

Rozemberczki, B., Allen, C., and Sarkar, R. Multi-scale attributed node embedding. *arXiv preprint arXiv:1909.13021*, 2019.

Satorras, V. G. and Estrach, J. B. Few-shot learning with graph neural networks. In *International Conference on Learning Representations*, 2018.

Sen, P., Namata, G., Bilgic, M., Getoor, L., Galligher, B., and Eliassi-Rad, T. Collective classification in network data. *AI magazine*, 29(3):93–93, 2008.

Shchur, O., Mumme, M., Bojchevski, A., and Günnemann, S. Pitfalls of graph neural network evaluation. *Relational Representation Learning Workshop, NeurIPS 2018*, 2018.

Shi, Z., Swersky, K., Tarlow, D., Ranganathan, P., and Hashemi, M. Learning execution through neural code fusion. In *International Conference on Learning Representations*, 2019.

Tang, J., Sun, J., Wang, C., and Yang, Z. Social influence analysis in large-scale networks. In *Proceedings of the 15th ACM SIGKDD international conference on Knowledge discovery and data mining*, pp. 807–816, 2009.

Veličković, P., Cucurull, G., Casanova, A., Romero, A., Lio, P., and Bengio, Y. Graph attention networks. *arXiv preprint arXiv:1710.10903*, 2017.

Veličković, P., Buesing, L., Overlan, M., Pascanu, R., Vinyals, O., and Blundell, C. Pointer graph networks. *Advances in Neural Information Processing Systems*, 33, 2020.

Wang, G., Ying, R., Huang, J., and Leskovec, J. Improving graph attention networks with large margin-based constraints. *arXiv preprint arXiv:1910.11945*, 2019.

Xu, K., Hu, W., Leskovec, J., and Jegelka, S. How powerful are graph neural networks? In *International Conference on Learning Representations*, 2018a.

Xu, K., Li, C., Tian, Y., Sonobe, T., Kawarabayashi, K.-i., and Jegelka, S. Representation learning on graphs with jumping knowledge networks. In *International Conference on Machine Learning*, pp. 5453–5462. PMLR, 2018b.

Yan, Y., Zhu, J., Duda, M., Solarz, E., Sripada, C., and Koutra, D. Groupinn: Grouping-based interpretable neural network for classification of limited, noisy brain data. In *Proceedings of the 25th ACM SIGKDD International Conference on Knowledge Discovery & Data Mining*, pp. 772–782, 2019.

Yan, Y., Swersky, K., Koutra, D., Ranganathan, P., and Hashemi, M. Neural execution engines: Learning to execute subroutines. *Advances in Neural Information Processing Systems*, 33, 2020.

Zhao, L. and Akoglu, L. Pairnorm: Tackling oversmoothing in gnns. In *International Conference on Learning Representations*, 2019.

Zhou, K., Dong, Y., Wang, K., Lee, W. S., Hooi, B., Xu, H., and Feng, J. Understanding and resolving performance degradation in graph convolutional networks, 2020.

Zhu, J., Yan, Y., Zhao, L., Heimann, M., Akoglu, L., and Koutra, D. Beyond homophily in graph neural networks: Current limitations and effective designs. *Advances in Neural Information Processing Systems*, 33, 2020.

Zhu, J., Rossi, R. A., Rao, A., Mai, T., Lipka, N., Ahmed, N. K., and Koutra, D. Graph neural networks with heterophily. In *AAAI Conference on Artificial Intelligence*, 2021.

A. Detailed Proofs of Theorems in § 3

A.1. Proof of Theorem 1

Proof. Before the operation of $\tilde{\mathbf{A}}\mathbf{F}^0$, the distance between the mean vectors of the two classes is: $2\|\boldsymbol{\mu}\|$ and the variance within each class is $\boldsymbol{\Sigma}$. The smaller the distance between the two classes is, the less distinguishable the node features of the two classes are.

After this operation, the node representation of any node v_i is given by:

$$\mathbf{f}_i^1 = \frac{\mathbf{f}_i^0}{d_i + 1} + \sum_{j \in \mathcal{N}_i} \frac{\mathbf{f}_j^0}{\sqrt{d_i + 1} \cdot \sqrt{d_j + 1}}. \quad (13)$$

Without loss of generality, we assume node v_i is in the first class \mathcal{V}_1 and denote $\frac{|\mathcal{N}_i^s|}{|\mathcal{N}_i|}$ as k_i . Then, we can express the expectation of \mathbf{f}_i^1 as:

$$\mathbb{E}(\mathbf{f}_i^1) = \mathbb{E}(\mathbb{E}(\mathbf{f}_i^1 | k_i)) \quad (14)$$

$$\begin{aligned} \mathbb{E}(\mathbf{f}_i^1 | k_i) &= \mathbb{E}\left(\frac{\mathbf{f}_i^0}{d_i + 1} | k_i\right) + \sum_{j \in \mathcal{N}_i} \mathbb{E}\left(\frac{\mathbf{f}_j^0}{\sqrt{d_i + 1} \cdot \sqrt{d_j + 1}} | k_i\right) \\ &= \frac{\boldsymbol{\mu}}{d_i + 1} + \sum_{j \in \mathcal{N}_i} \left(\mathbb{E}\left(\frac{\mathbf{f}_j^0}{\sqrt{d_i + 1} \cdot \sqrt{d_j + 1}} | k_i, v_j \in \mathcal{V}_1\right) \cdot \mathbb{P}(v_j \in \mathcal{V}_1 | k_i) \right. \\ &\quad \left. + \mathbb{E}\left(\frac{\mathbf{f}_j^0}{\sqrt{d_i + 1} \cdot \sqrt{d_j + 1}} | k_i, v_j \in \mathcal{V}_2\right) \cdot \mathbb{P}(v_j \in \mathcal{V}_2 | k_i) \right) \\ &= \frac{\boldsymbol{\mu}}{d_i + 1} + \sum_{j \in \mathcal{N}_i} \left(\frac{k_i}{\sqrt{d_i + 1} \cdot \sqrt{d_j + 1}} \boldsymbol{\mu} - \frac{(1 - k_i)}{\sqrt{d_i + 1} \cdot \sqrt{d_j + 1}} \boldsymbol{\mu} \right) \\ &= \frac{\boldsymbol{\mu}}{d_i + 1} + \frac{(2k_i - 1)\boldsymbol{\mu}}{\sqrt{d_i + 1}} \sum_{j \in \mathcal{N}_i} \frac{1}{\sqrt{d_j + 1}}. \end{aligned} \quad (15)$$

Given $\mathbb{E}(k_i) = h$, Equation (14) and Equation (15), we have:

$$\begin{aligned} \mathbb{E}(\mathbf{f}_i^1) &= \mathbb{E}\left(\frac{\boldsymbol{\mu}}{d_i + 1} + \frac{(2k_i - 1)\boldsymbol{\mu}}{\sqrt{d_i + 1}} \sum_{j \in \mathcal{N}_i} \frac{1}{\sqrt{d_j + 1}}\right) \\ &= \frac{\boldsymbol{\mu}}{d_i + 1} + \frac{(2h_i - 1)\boldsymbol{\mu}}{\sqrt{d_i + 1}} \sum_{j \in \mathcal{N}_i} \frac{1}{\sqrt{d_j + 1}} \\ &= \left(\frac{1}{d_i + 1} + \frac{\sum_{j \in \mathcal{N}_i} \frac{1}{\sqrt{d_j + 1}}}{\sqrt{d_i + 1}} (2h_i - 1) \right) \boldsymbol{\mu} \\ &= \left(\frac{1}{d_i + 1} + \frac{\sum_{j \in \mathcal{N}_i} \frac{\sqrt{d_i + 1}}{\sqrt{d_j + 1}}}{d_i + 1} (2h_i - 1) \right) \boldsymbol{\mu} \\ &= \left(\frac{1 + (2h_i - 1)d_i \bar{r}_i}{d_i + 1} \right) \boldsymbol{\mu} \equiv \gamma_i^0 \boldsymbol{\mu}. \end{aligned} \quad (16)$$

Where $\bar{r}_i \equiv \frac{1}{d_i} \sum_{j \in \mathcal{N}_i} \frac{\sqrt{d_i + 1}}{\sqrt{d_j + 1}}$.

Next, we consider three cases: (1) $h_i \leq 0.5$, (2) $h_i > 0.5$ & $\bar{r}_i \leq \frac{1}{\epsilon}$, and (3) $h_i > 0.5$ & $\bar{r}_i > \frac{1}{\epsilon}$.

- **CASE 1: $h_i \leq 0.5$**

- **Upper Bound**

We have:

$$\gamma_i^0 \leq \frac{1}{d_i + 1} \leq \frac{1}{2}. \quad (17)$$

- **Lower Bound**

To see if there exists a lower bound, we first show that when $h_i \leq 0.5$, $\frac{1+(2h_i-1)d_i\bar{r}_i}{d_i+1}$ is a decreasing function of d_i given that $d_i \geq 1$.

When $h_i \leq 0.5$, we have:

1. $(2h_i - 1)d_i \leq 0$
2. $\frac{d_i}{d_i+1}$ is an increasing function of d_i
3. \bar{r}_i is an increasing function of d_i
4. $\frac{1}{d_i+1}$ is a decreasing function of d_i

Thus $\frac{1+(2h_i-1)d_i\bar{r}_i}{d_i+1}$ is a decreasing function of d_i .

When $h_i = 0.5$, $\frac{1+(2h_i-1)d_i\bar{r}_i}{d_i+1} = \frac{1}{d_i+1}$ and $0 < \frac{1}{d_i+1} \leq \frac{1}{2}$.

When $h_i < 0.5$,

$$\begin{aligned} \frac{1+(2h_i-1)d_i\bar{r}_i}{d_i+1} &\leq \frac{(2h_i-1)d_i\bar{r}_i}{d_i+1} + \frac{1}{2} \\ &\leq \frac{(2h_i-1)\bar{r}_i}{2} + \frac{1}{2}. \end{aligned} \quad (18)$$

And we know that when $h_i < 0.5$:

$$\lim_{d_i \rightarrow \infty} \frac{(2h_i-1)\bar{r}_i}{2} + \frac{1}{2} = -\infty. \quad (19)$$

Thus,

$$\lim_{d_i \rightarrow \infty} \frac{1+(2h_i-1)d_i\bar{r}_i}{d_i+1} = -\infty. \quad (20)$$

- **CASE 2: $h_i > 0.5$ & $\bar{r}_i \leq \frac{1}{\epsilon}$**

For $h_i > 0.5$, let $\epsilon = 2h_i - 1$ and $0 < \epsilon \leq 1$. Then, we have:

$$\mathbb{E}(\mathbf{f}_i^1) = \left(\frac{1 + \epsilon d_i \bar{r}_i}{d_i + 1} \right) \boldsymbol{\mu}. \quad (21)$$

If $\bar{r}_i \leq \frac{1}{\epsilon}$, then $0 < \epsilon \bar{r}_i \leq 1$, so $\frac{1}{2} < \gamma_i^0 \leq 1$.

- **CASE 3: $h_i > 0.5$ & $\bar{r}_i > \frac{1}{\epsilon}$**

In this case, Equation (21) still holds, since $h_i > 0.5$.

- **Lower Bound**

If $\bar{r}_i > \frac{1}{\epsilon}$, then $\epsilon \bar{r}_i > 1$ and therefore $\gamma_i^0 > 1$.

- **Upper Bound**

When $\epsilon > 0$,

$$\begin{aligned} \frac{1 + \epsilon d_i \bar{r}_i}{d_i + 1} &> \frac{\epsilon d_i \bar{r}_i}{d_i + 1} \\ &\geq \frac{\epsilon \bar{r}_i}{2}. \end{aligned} \quad (22)$$

Because

$$\lim_{d_i \rightarrow \infty} \frac{\epsilon \bar{r}_i}{2} = \infty, \quad (23)$$

we have:

$$\lim_{d_i \rightarrow \infty} \frac{1 + \epsilon d_i \bar{r}_i}{d_i + 1} = \infty. \quad (24)$$

To sum it up,

$$\gamma_i^0 \in \begin{cases} (-\infty, \frac{1}{2}], & \text{if } h_i \leq 0.5 \\ (\frac{1}{2}, 1], & \text{if } h_i > 0.5 \text{ \& } \bar{r}_i \leq \frac{1}{2h_i - 1} \\ (1, \infty), & \text{otherwise.} \end{cases} \quad (25)$$

Remarks: Special cases

For different types of graphs and different nodes in the graph, $d_i \bar{r}_i$ might be different. For a **d-regular graph** whose nodes have constant degree or a graph whose adjacency matrix is **row-normalized**, we will have:

$$\begin{aligned} \gamma_i^0 &= \left(\frac{1 + (2h_i - 1)d_i \bar{r}_i}{d_i + 1} \right) \\ &\leq \left(\frac{1}{(d_i + 1)} + \frac{d_i}{(d_i + 1)} \right) = 1 \end{aligned} \quad (26)$$

Equality is achieved if and only if $h_i = 1$. To note that, $h_i = 1$ is not achievable for every node as long as there are more than one class. **Boundary nodes** will suffer most.

Then, we will take a look at the variance within each class. If we assume that the feature vectors are independent of each other, then we will have:

$$\begin{aligned} \mathbb{V}(\mathbf{f}_i^1) &= \mathbb{V} \left(\frac{\mathbf{f}_i^0}{d_i + 1} \right) + \sum_{j \in \mathcal{N}_i} \mathbb{V} \left(\frac{\mathbf{f}_j^0}{\sqrt{d_i + 1} \cdot \sqrt{d_j + 1}} \right) \\ &= \left(\frac{1}{(d_i + 1)^2} + \sum_{j \in \mathcal{N}_i} \frac{1}{(d_i + 1)(d_j + 1)} \right) \Sigma \\ &= \frac{1}{d_i + 1} \left(\frac{1}{d_i + 1} + \sum_{j \in \mathcal{N}_i} \frac{1}{d_j + 1} \right) \Sigma \end{aligned} \quad (27)$$

$$\frac{1}{d_i + 1} \left(\frac{1}{d_i + 1} + \sum_{j \in \mathcal{N}_i} \frac{1}{d_j + 1} \right) \leq \frac{1}{2} \quad (28)$$

Note that we can derive similar results for any node v_t in the second class.

From Equation 27, we can have the following conclusion:

$\tilde{\mathbf{A}}\mathbf{F}^0$ will reduce the variance of the node feature distribution and the reduction is irrelevant to the homophily h_i . The larger degree of the node, the greater the reduction will be in the variance. Note that the reduction of the variance of each node does not mean the reduction of the variance of the class as a whole. When the degree and the homophily of the nodes are diverse, the variance of the class can increase. \square

A.2. Proof of Theorem 3

Proof. Similar to Equation 14, we can express the expectation of \mathbf{f}_i^1 as:

$$\begin{aligned}
 \mathbb{E}(\mathbf{f}_i^1) &= \mathbb{E}(\mathbb{E}(\mathbf{f}_i^1 | m_i^0)) \\
 &= \mathbb{E} \left(\mathbb{E} \left(\frac{\mathbf{f}_i^0}{d_i + 1} | m_i^0 \right) + \sum_{j \in \mathcal{N}_i} \mathbb{E} \left(\frac{\mathbf{f}_j^0}{\sqrt{d_i + 1} \cdot \sqrt{d_j + 1}} | m_i^0 \right) \right) \\
 &= \mathbb{E} \left(\frac{\boldsymbol{\mu}}{d_i + 1} + \sum_{j \in \mathcal{N}_i} \left(\mathbb{E} \left(\frac{\mathbf{f}_j^0}{\sqrt{d_i + 1} \cdot \sqrt{d_j + 1}} | m_i^0, v_j \in \mathcal{V}_1 \right) \mathbb{P}(v_j \in \mathcal{V}_1 | m_i^0) \right. \right. \\
 &\quad \left. \left. + \mathbb{E} \left(\frac{\mathbf{f}_j^0}{\sqrt{d_i + 1} \cdot \sqrt{d_j + 1}} | m_i^0, v_j \in \mathcal{V}_2 \right) \mathbb{P}(v_j \in \mathcal{V}_2 | m_i^0) \right) \right). \tag{29}
 \end{aligned}$$

Next, we will show how to compute the conditional expectation and conditional probability in the summand.

$$\begin{aligned}
 \mathbb{E} \left(\frac{\mathbf{f}_j^0}{\sqrt{d_i + 1} \cdot \sqrt{d_j + 1}} | m_i^0, v_j \in \mathcal{V}_1 \right) &= \mathbb{E} \left(\frac{\mathbf{f}_j^0}{\sqrt{d_i + 1} \cdot \sqrt{d_j + 1}} | m_i^0, v_j \in \mathcal{V}_1, v_j \text{ wrongly send information} \right) \\
 &\quad \cdot \mathbb{P}(v_j \text{ wrongly send information} | m_i^0, v_j \in \mathcal{V}_1) \\
 &\quad + \mathbb{E} \left(\frac{\mathbf{f}_j^0}{\sqrt{d_i + 1} \cdot \sqrt{d_j + 1}} | m_i^0, v_j \in \mathcal{V}_1, v_j \text{ correctly send information} \right) \\
 &\quad \cdot \mathbb{P}(v_j \text{ correctly send information} | m_i^0, v_j \in \mathcal{V}_1). \tag{30}
 \end{aligned}$$

Combined with the conditional independence assumption, we have:

$$\begin{aligned}
 \mathbb{P}(v_j \text{ wrongly send information} | m_i^0, v_j \in \mathcal{V}_1) &= \frac{\mathbb{P}(v_j \text{ wrongly send information}, v_j \in \mathcal{V}_1 | m_i^0)}{\mathbb{P}(v_j \in \mathcal{V}_1 | m_i^0)} \\
 &= \frac{\mathbb{P}(v_j \text{ wrongly send information} | m_i^0) \cdot \mathbb{P}(v_j \in \mathcal{V}_1 | m_i^0)}{\mathbb{P}(v_j \in \mathcal{V}_1 | m_i^0)} \\
 &= \mathbb{P}(v_j \text{ wrongly send information} | m_i^0) = m_i^0. \tag{31}
 \end{aligned}$$

Similarly, we obtain:

$$\mathbb{P}(v_j \text{ correctly send information} | m_i^0, v_j \in \mathcal{V}_1) = 1 - m_i^0. \tag{32}$$

Then Equation (30) can be rewritten as:

$$\begin{aligned}
 \mathbb{E} \left(\frac{\mathbf{f}_j^0}{\sqrt{d_i + 1} \cdot \sqrt{d_j + 1}} | m_i^0, v_j \in \mathcal{V}_1 \right) &= \mathbb{E} \left(\frac{\mathbf{f}_j^0}{\sqrt{d_i + 1} \cdot \sqrt{d_j + 1}} | m_i^0, v_j \in \mathcal{V}_1, v_j \text{ wrongly send information} \right) \cdot m_i^0 \\
 &\quad + \mathbb{E} \left(\frac{\mathbf{f}_j^0}{\sqrt{d_i + 1} \cdot \sqrt{d_j + 1}} | m_i^0, v_j \in \mathcal{V}_1, v_j \text{ correctly send information} \right) \cdot (1 - m_i^0) \\
 &= - \frac{m_i^0 \boldsymbol{\mu}}{\sqrt{d_i + 1} \cdot \sqrt{d_j + 1}} + \frac{(1 - m_i^0) \boldsymbol{\mu}}{\sqrt{d_i + 1} \cdot \sqrt{d_j + 1}} \\
 &= \frac{(1 - 2m_i^0) \boldsymbol{\mu}}{\sqrt{d_i + 1} \cdot \sqrt{d_j + 1}}. \tag{33}
 \end{aligned}$$

Similarly, we have:

$$\mathbb{E} \left(\frac{\mathbf{f}_j^0}{\sqrt{d_i + 1} \cdot \sqrt{d_j + 1}} | m_i^0, v_j \in \mathcal{V}_2 \right) = \frac{(1 - 2m_i^0) \boldsymbol{\mu}}{\sqrt{d_i + 1} \cdot \sqrt{d_j + 1}}. \tag{34}$$

Consider the independence between m_i^0 and node class, and insert Equation (33) and Equation (34) into Equation (29), we will have:

$$\begin{aligned}
 \mathbb{E}(\mathbf{f}_i^1) &= \mathbb{E} \left(\frac{\boldsymbol{\mu}}{d_i + 1} + \sum_{j \in \mathcal{N}_i} \left(\frac{(1 - 2m_i^0)k_i \boldsymbol{\mu}}{\sqrt{d_i + 1} \cdot \sqrt{d_j + 1}} + \frac{(1 - 2m_i^0)(1 - k_i) \boldsymbol{\mu}}{\sqrt{d_i + 1} \cdot \sqrt{d_j + 1}} \right) \right) \\
 &= \mathbb{E} \left(\frac{\boldsymbol{\mu}}{d_i + 1} + \sum_{j \in \mathcal{N}_i} \frac{(1 - 2m_i^0) \boldsymbol{\mu}}{\sqrt{d_i + 1} \cdot \sqrt{d_j + 1}} \right) \\
 &= \frac{\boldsymbol{\mu}}{d_i + 1} + \sum_{j \in \mathcal{N}_i} \frac{(1 - 2e_i^0) \boldsymbol{\mu}}{\sqrt{d_i + 1} \cdot \sqrt{d_j + 1}} \\
 &= \left(\frac{1 + (1 - 2e_i^0) d_i \bar{r}_i}{d_i + 1} \right) \boldsymbol{\mu} \equiv \gamma_i^0 \mathbb{E}(\mathbf{f}_i^0).
 \end{aligned} \tag{35}$$

The ranges of γ_i^0 under different conditions of e_i^0 and \bar{r}_i can be derived similarly as shown by the Proof A.1. \square

B. Additional Experiments

B.1. Batch norm & Layer norm

As mentioned in §4.4, our theorems predict that batch norm and layer norm will help alleviate oversmoothing, but they will also decrease the accuracy in the supervised node classification task. This phenomenon is more prominent in the heterophily datasets. In this section, we verify this conjecture by comparing the prediction accuracy of the base model with models that use either batch norm or layer norm. We use the following base model (the same model used in §5.4): a GCN (Kipf & Welling, 2016) with weight bias, Elu non-linearity and residual connection. We do **not** include any of our designs so as to exclude any other factors that can affect the performance. The models we compare against are +BN and +LN, which represent the models that add batch norm and layer norm right before the non-linear activation, respectively.

Table B.1. Effects of using batch norm & layer norm: decrease in accuracy but improvement in oversmoothing. Best performance of each model across different layers is highlighted in gray.

Layers	2	4	8	16	32	64	2	4	8	16	32	64
Cora ($h=0.81$)												
Base	86.56 \pm 1.21	86.04 \pm 0.72	85.51 \pm 1.51	85.33 \pm 0.72	85.37 \pm 1.58	72.17 \pm 8.89	76.51 \pm 1.63	75.03 \pm 1.67	73.96 \pm 1.52	73.59 \pm 1.51	71.91 \pm 1.94	32.08 \pm 15.74
+BN	84.73 \pm 1.10	83.76 \pm 1.61	83.94 \pm 1.51	84.57 \pm 1.22	84.63 \pm 1.58	85.17 \pm 1.18	71.62 \pm 1.48	71.58 \pm 1.00	72.18 \pm 1.39	72.45 \pm 1.42	72.76 \pm 1.31	72.61 \pm 1.41
+LN	84.73 \pm 1.63	86.60 \pm 1.01	86.72 \pm 1.36	86.08 \pm 1.16	85.67 \pm 1.23	85.13 \pm 1.20	76.11 \pm 1.80	74.02 \pm 2.77	75.00 \pm 1.95	74.50 \pm 0.96	74.49 \pm 2.10	73.94 \pm 2.03
Citeseer ($h=0.74$)												
Base	61.89 \pm 3.72	60.00 \pm 5.24	58.92 \pm 5.24	56.49 \pm 5.73	58.92 \pm 3.15	49.19 \pm 16.70	64.98 \pm 1.84	62.65 \pm 3.09	62.43 \pm 3.28	54.69 \pm 2.58	47.68 \pm 2.63	29.74 \pm 5.21
+BN	58.38 \pm 6.42	59.19 \pm 4.59	55.41 \pm 6.65	57.30 \pm 3.15	57.57 \pm 6.29	57.02 \pm 6.19	60.88 \pm 2.24	61.38 \pm 2.17	61.84 \pm 4.08	61.97 \pm 3.01	59.04 \pm 3.79	57.84 \pm 3.67
+LN	58.11 \pm 6.19	55.68 \pm 6.19	58.92 \pm 7.63	59.19 \pm 3.07	58.92 \pm 3.15	58.00 \pm 3.03	61.86 \pm 1.73	62.17 \pm 2.48	62.41 \pm 2.99	60.37 \pm 2.36	58.25 \pm 3.03	58.92 \pm 3.15
Cornell ($h=0.3$)												
Base	61.89 \pm 3.72	60.00 \pm 5.24	58.92 \pm 5.24	56.49 \pm 5.73	58.92 \pm 3.15	49.19 \pm 16.70	64.98 \pm 1.84	62.65 \pm 3.09	62.43 \pm 3.28	54.69 \pm 2.58	47.68 \pm 2.63	29.74 \pm 5.21
+BN	58.38 \pm 6.42	59.19 \pm 4.59	55.41 \pm 6.65	57.30 \pm 3.15	57.57 \pm 6.29	57.02 \pm 6.19	60.88 \pm 2.24	61.38 \pm 2.17	61.84 \pm 4.08	61.97 \pm 3.01	59.04 \pm 3.79	57.84 \pm 3.67
+LN	58.11 \pm 6.19	55.68 \pm 6.19	58.92 \pm 7.63	59.19 \pm 3.07	58.92 \pm 3.15	58.00 \pm 3.03	61.86 \pm 1.73	62.17 \pm 2.48	62.41 \pm 2.99	60.37 \pm 2.36	58.25 \pm 3.03	58.92 \pm 3.15
Chameleon ($h=0.23$)												
Base	61.89 \pm 3.72	60.00 \pm 5.24	58.92 \pm 5.24	56.49 \pm 5.73	58.92 \pm 3.15	49.19 \pm 16.70	64.98 \pm 1.84	62.65 \pm 3.09	62.43 \pm 3.28	54.69 \pm 2.58	47.68 \pm 2.63	29.74 \pm 5.21
+BN	58.38 \pm 6.42	59.19 \pm 4.59	55.41 \pm 6.65	57.30 \pm 3.15	57.57 \pm 6.29	57.02 \pm 6.19	60.88 \pm 2.24	61.38 \pm 2.17	61.84 \pm 4.08	61.97 \pm 3.01	59.04 \pm 3.79	57.84 \pm 3.67
+LN	58.11 \pm 6.19	55.68 \pm 6.19	58.92 \pm 7.63	59.19 \pm 3.07	58.92 \pm 3.15	58.00 \pm 3.03	61.86 \pm 1.73	62.17 \pm 2.48	62.41 \pm 2.99	60.37 \pm 2.36	58.25 \pm 3.03	58.92 \pm 3.15

Table B.1 shows that both batch norm and layer norm can help with oversmoothing. Moreover, adding layer norm is in general better than adding batch norm. This is expected because the scaling effect caused by the propagation can be alleviated by normalizing across the node features. Thus, the dispersion of the expected feature vectors can be mitigated. On the other hand, batch norm normalizes across all the nodes, so it requires sacrificing the nodes that benefit (case 3) to compensate for the nodes that are prone to moving towards the other classes (case 1 & case 2). As a result, batch norm is less effective in mitigating oversmoothing and leads to a bigger decrease in accuracy.

Another finding is that both layer norm and batch norm lead to a significant accuracy decrease (2%-3%) in the heterophily datasets. +BN has a clear accuracy drop even in the homophily datasets. As Thm. 1 points out: higher heterophily level may result in sign flip. If the features flip the sign, using batch norm or layer norm will not revert the sign, but they may instead encourage the features to move towards the other class more.

Given the limitations shown above, we do **not** use either batch norm or layer norm in our proposed model, GGCN.

B.2. More on the Initial & Developing Stages

Section 5.5 shows how the node classification accuracy changes for nodes of different degrees with the number of layers on Citeseer. Here, we provide more details of this experiment and give the results on another dataset, Cora.

Datasets. According to Thm. 1 and 2, in order to see both the initial and the developing stage, we need to use homophily datasets. Recall that in heterophily data, $\hat{h}_i < 0.5$ for all the nodes, so the initial stage does not exist and only case 2 applies.

Measurement of effective homophily \hat{h}_i . In a multi-class setting, effective homophily \hat{h}_i is defined as the portion of neighbors whose features are inside the decision boundary of class $\chi(v_i)$. To align this with our theorems—which apply to binary classification—the decision boundary is defined as the curve that maximizes the margins between the initial features in different classes. In binary classification, the decision boundary is the origin.

To estimate the effective homophily \hat{h}_i , we measure the portion of neighbors that have the same ground truth label as v_i and are correctly classified. We use this ratio to approximate the neighbors whose features are still inside the decision boundary of class $\chi(v_i)$. Following our theory, we estimate \hat{h}_i before the last propagation takes place and analyze its impact on the accuracy of the final layer. In more detail, we obtain the node features before the last propagation from a trained vanilla GCN (Kip & Welling, 2016) and then perform a linear transformation using the weight matrix and bias vector from the last layer. Then, we use the transformed features to classify the neighbors of node v_i and compute \hat{h}_i . We note that we leverage the intermediate features only for the estimation of \hat{h}_i ; the accuracy of the final layer is still measured using the outputs from the final layer.

Degree intervals. To investigate the change in GNN accuracy with different layers for nodes with different degrees, we categorize the nodes in n degree intervals. For the degree intervals, we use logarithmic binning (base 2). In detail, we denote the highest and lowest degree by d_{max} and d_{min} , respectively, and let $\Omega \equiv \frac{\log_2 d_{max} - \log_2 d_{min}}{n}$. Then, we divide the nodes into n intervals, where the j -th interval is defined as: $[d_{min} \cdot 2^{(j-1)\Omega}, d_{min} \cdot 2^{j\Omega})$.

Dataset: Citeseer. Figure 2 and Table B.2 show how the accuracy changes with the number of layers for different node degree intervals. We observe that in the initial stage (when $\hat{h}_i > 0.5$), the accuracy increases as the degree and \hat{h}_i increase. However, in the developing stage ($\hat{h}_i \leq 0.5$), the accuracy of high-degree nodes drops more sharply than that of low-degree nodes.

Dataset: Cora. The results for Cora are shown in Figure B.1 and Table B.3. In the initial stage, the nodes with lower

Table B.2. Citeseer: Accuracy (Acc) and average effective homophily (\bar{h}_i) for nodes with different degrees across various layers. Last layer of initial stage ($\hat{h}_i > 0.5 \forall$ degree) marked in gray.

Layers	Degrees				
	[1, 2]	[3, 6]	[7, 15]	[16, 39]	[40, 99]
2	Acc	74.44	78.51	84.04	96.00
	\bar{h}_i	0.65	0.67	0.72	0.83
3	Acc	70.92	77.59	83.03	92.75
	\bar{h}_i	0.63	0.66	0.71	0.84
4	Acc	60.54	68.56	77.63	94.00
	\bar{h}_i	0.54	0.58	0.66	0.79
5	Acc	41.66	48.70	56.97	61.33
	\bar{h}_i	0.36	0.38	0.45	0.48
6	Acc	23.61	28.87	41.17	31.83
	\bar{h}_i	0.18	0.19	0.27	0.22

Table B.3. Cora: Accuracy and average effective homophily (\bar{h}_i) for nodes with different degrees across different layers. Last layer of initial stage ($\hat{h}_i > 0.5 \forall$ degree) marked in gray.

Layers	Degrees				
	[1, 2]	[3, 7]	[8, 21]	[22, 60]	[61, 168]
2	Acc	85.14	88.52	83.78	90.00
	\bar{h}_i	0.77	0.77	0.72	0.63
3	Acc	82.28	87.26	84.42	85.00
	\bar{h}_i	0.77	0.78	0.73	0.64
4	Acc	79.57	85.52	83.26	85.00
	\bar{h}_i	0.75	0.76	0.71	0.63
5	Acc	77.38	83.75	82.83	85.00
	\bar{h}_i	0.72	0.73	0.68	0.56
6	Acc	63.35	68.20	66.01	70.00
	\bar{h}_i	0.57	0.60	0.54	0.52
7	Acc	30.91	30.62	29.12	17.50
	\bar{h}_i	0.25	0.26	0.21	0.26
8	Acc	31.48	31.02	28.44	32.50
	\bar{h}_i	0.24	0.26	0.20	0.28

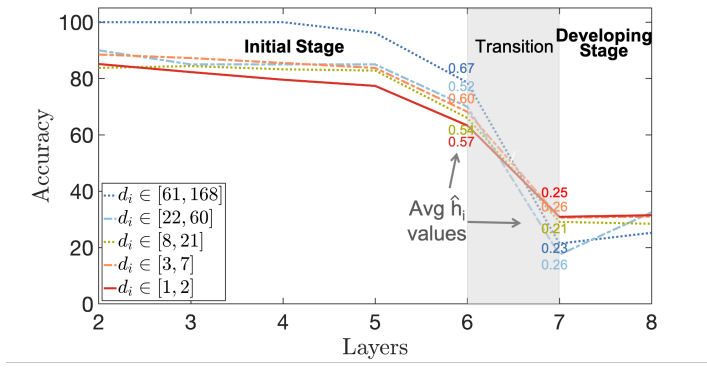


Figure B.1. Cora: Accuracy per (logarithmic) degree bin.

degrees usually have lower accuracy. One exception is the nodes with degrees in the range [3, 7]. These nodes have higher accuracy because the average effective homophily \bar{h}_i of that degree group is the second highest. In the developing stage, the accuracy of the high-degree nodes drops more than the accuracy of the remaining node groups.

GCN's behavior on both Citess and Cora datasets verifies our conjecture based on our theorems in § 3.1.

B.3. Hyperparameter Settings

Experiments for Table 1 & Table 2

For the baselines, we set the same hyperparameters that are provided by the original papers or the authors' github repositories, and we match the results they reported in their respective papers. In our experiments, we find that the original hyperparameters set by the authors are already well-tuned.

All the models use Adam as the optimizer. GAT sets the initial learning rate as 0.005 and Geom-GCN uses a custom learning scheduler. All the other models (include GGCN) use the initial learning rate 0.01.

For GGCN, we use the following hyperparameters:

- k in the decaying aggregation: 3
- Initialization of λ_0^l and λ_1^l : 0.5 and 0, respectively
- Initialization of $\alpha^l, \beta_0^l, \beta_1^l$ and β_2^l : 2, 0, 0, 0, respectively.

We tune the parameters in the following ranges:

- Dropout rate: [0.0, 0.7]
- Weight decay: [1e-7, 1e-2]
- Hidden units: {8, 16, 32, 64, 80}
- Decay rate η : [0.0, 1.5]

Experiments for Table 3 and Table B.1

The hyperparameters that are used in all the models (Base, +deg, +sign, +deg, sign, +BN, +LN) are set to be the same and they are tuned for every dataset. Those common hyperparameters are:

- Dropout rate: [0.0, 0.7]
- Weight decay: [1e-7, 1e-2]
- Hidden units: {8, 16, 32, 64, 80}

For models that use signed messages, we tune the following hyperparameter:

- Initialization of α^l : [0.2, 1.0] (same in every layer)

For models that use degree correction, we tune the following hyperparameter:

- Initialization of λ_0^l : [0.2, 1.5] (same in every layer)